Supplementary Information

1. Bed topography digital elevation model

Bed topography across the study area is derived from a detailed aerogeophysical survey (Fig. 1A, black lines) of the Institute and Möller Ice Streams (IMIS) and a series of individual flightlines flown in the 1970s (Fig. 1A, black dashed lines). Bedmap2 provides a grid of Antarctica's bed topography that incorporates these datasets, but does not provide access to the raw data (Fretwell et al., 2013). Although the data is rendered at a 1 km resolution, Bedmap2 bed topography is only really effective at a 5 km grid resolution due to the distribution of direct measurements (Fretwell et al., 2013). This work, however, is funded by the NERC AFI project that surveyed the IMIS. Therefore, the raw flightline data can be used in the gridding process, rather than the Bedmap2 data, in order to produce a more detailed grid of subglacial topography for this region. This was achieved using standard geoprocessing tools in the Spatial Analyst Toolbox in ArcGIS, as outlined below.

The IMIS flightline data records elevations relative to WGS84. Therefore, a correction was applied to Bedmap2 to convert elevations from meters relative to sea level as defined by the g104c geoid to WGS84 datum heights. This involved subtracting the correction grid provided from the Bedmap2 grid (Fretwell et al., 2013). A section of the grid, encompassing the study area under investigation (Fig. 1), was then extracted from Bedmap2 and converted to points. Each point represents the bed elevation value at the centre of a 5 km grid cell. A cubic convolution algorithm was used to determine this elevation. Bedmap2 elevation data were then deleted where they coincide with IMIS flightline data. The IMIS survey points are then gridded with the Bedmap2 points for the study area, at a 1 km resolution, using the 'Topo to Raster' function in ArcGIS. This uses an iterative finite difference interpolation technique that employs a nested grid strategy to calculate successively finer grids until the user specified resolution is obtained (Hutchinson 1988a,b). This technique has been widely used as the algorithm has been shown to represent glaciated landscapes well and was employed in the creation of Bedmap2 (Fretwell et al., 2013). The resulting grid was used as the basis of analysis for this paper, except where it was possible to use bed elevations directly from the IMIS flightline data (e.g. channel cross-profiles).

2. MODIS MOA image map

The Moderate Resolution Imaging Spectroradiometer (MODIS) comprises visible and near-infrared satellite sensors, which measure brightness variations in Bands 1 and 2. The Mosaic of Antarctic (MOA) image map (2004) consists of 260 MODIS orbit swaths, and represents a composite of digitally smoothed red-light (MODIS Band 1) images, at a resolution of 125 m (Haran et al., 2005, updated 2013). The processing steps involved mean that the final image is a consistent and semi-quantitative representation of red-light reflections. Brightness variations in the image radiometry produce a detailed picture of the morphology of the ice sheet surface (Scambos et al., 2007). This, in turn, provides information on ice flow, subglacial bedrock form, wind-derived features and the location of the ice sheet grounding line.

3. Extracting channel long-profiles

A total of 44 discontinuous linear features were identified in satellite imagery (Fig. 1; Fig. DR4). These were interpreted as the surface expression of channel segments in the underlying bed topography. In order to determine the long-profile elevations of these channel segments, their locations in MODIS MOA satellite imagery (Haran et al., 2005, updated 2013) were first digitised in ArcGIS (Fig. DR4A, green lines). Once digitised, the pattern and spatial connectivity between channel segments became more evident. For some channels and over short distances, it was possible to extrapolate between channel segments with confidence and, therefore, to reclassify these segments as one channel. This resulted in the classification of a total of 32 single channels (Fig. DR4B). The location and length of each digitised channel was recorded. Then, in order to determine the channel long-profile elevations, each channel segment was converted into equally spaced points, at 1 km intervals along each line. Bed elevations at each point were then sampled directly from the flightline data (where the two intersected) or from the grid of subglacial topography (see Supplementary Information #1). The long-profiles presented in Fig. DR5 are plots of these elevation values against distance along the segment length. The first point (0 km) is always the most southerly, with each subsequent point located further north, towards the grounding line, with distance along the profile. The black dots mark where bed elevations were taken from intersecting flightline data. The dashed lines show where channel segments were grouped to represent a single channel long-profile.

4. Determining hydrological potential

Hydrological potential represents the gradient along which water will flow under ice (Shreve, 1972; Cuffey and Paterson, 2010). This incorporates flow resulting from a combination of elevation and pressure gradients (high to low). As such hydrological potential (ϕ_h) can be defined as:

$$\emptyset_h = P_w + (\rho_w * g * z)$$

Where water density (ρ_w) is 1000 kg m^{-3}, gravitational acceleration (g) is 9.81 m s^{-2}, elevation (z) is taken from the bed elevation grid and subglacial water pressure (P_w) is assumed to be equivalent to ice overburden pressure (σ), as follows:

$$\sigma = \rho_i * g * h_i$$

where ρ_i is density of ice (917 kg m^{-3}), g is gravitational acceleration and h_i is ice thickness. This allows hydrological potential to be re-written (Shreve, 1972) as:

$$\emptyset_h = \sigma + (\rho_w * g * z)$$

In order to solve this equation two grids are created in ArcGIS, as follows:

$$GridA = \rho_i * g * h_i$$

$$GridB = \rho_w * g * z$$

The ice thickness and bed elevation values used in these calculations are derived from Bedmap2 grids (1 km resolution) (Fretwell et al., 2013). The hydrological potential gradient is then determined by adding these two grids together, resulting in 1 km gridded surface of hydrological potential.

This hydrological potential grid is then employed as the primary input to ArcGIS's Hydrology Toolbox, which is used to determine the flow of water across a surface and thereby, derive the hydrological potential flow paths. In this process, flow direction is determined, hydrological sinks are identified, flow accumulation is calculated (number of upslope cells flowing to a location) and hydrological networks are identified. These pathways represent where water would flow, if present, beneath the ice sheet (Fig. DR6).

References

Fretwell, P., *et al.* 2013, Bedmap2: improved ice bed, surface and thickness datasets for Antarctica: The Cryosphere, v. 7, p. 375-393.

Hutchinson, M. F., 1988a, Calculation of hydrologically sound digital elevation models, *in* Proceedings of the Third International Symposium on Spatial Data Handling, p. 117–133.

Hutchinson, M. F., 1988b, A new procedure for gridding elevation and streamline data with automatic removal of spurious pits: Journal of Hydrology, v. 106, p. 211–232.

Haran, T., Bohlander, J., Scambos, T., Painter, T., and Fahnestock, M., 2005, updated 2013, MODIS Mosaic of Antarctica (MOA) Image Map [NSIDC_0280, MOA125_2004]: Boulder, Colorado USA: National Snow and Ice Data Center, http://dx.doi.org/10.7265/N5ZK5DM5.

Scambos, T.A., Haran, T M., Fahnestock, M.A., Painter, T.H, and Bohlander, J., 2007, MODIS-based Mosaic of Antarctica (MOA) data sets: Continent-wide surface morphology and snow grain size: Remote Sensing of Environment, v. 111, no. 2-3, p. 242-257.

Shreve, R.L., 1972, Movement of water in glaciers: Journal of Glaciology, v. 11, no. 2, p. 205-214.

Cuffey K.M., and Patterson, W.S.B., 2010, The Physics of Glaciers (4th Edition): Butterworth-Heinemann, Oxford, UK.

Rignot, E., Mouginot, J., and Scheuchl, B., 2011, Ice flow of the Antarctic Ice Sheet: Science, v. 333, p. 1437-1430.

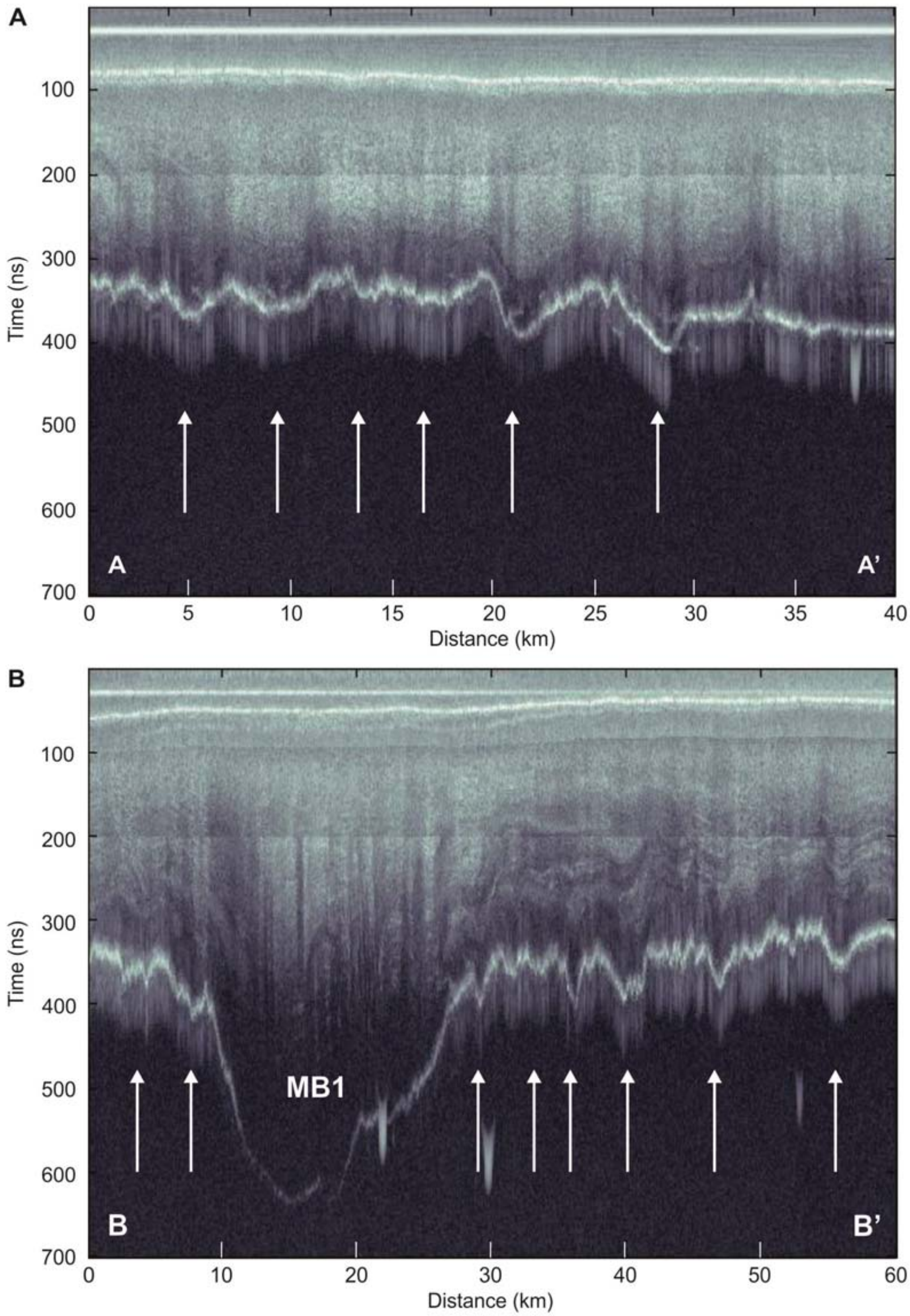

Figure DR1. Radar echograms showing examples of the subglacial channels identified. **A**: Radar echogram of transect A-A'. **B:** Radar echogram of transect B-B', which crosses the most northerly (down glacier) Marginal Basin 1. White arrows mark channel locations and correspond to the vertical dashed lines shown in the respective transects in Supplementary Fig. DR2.

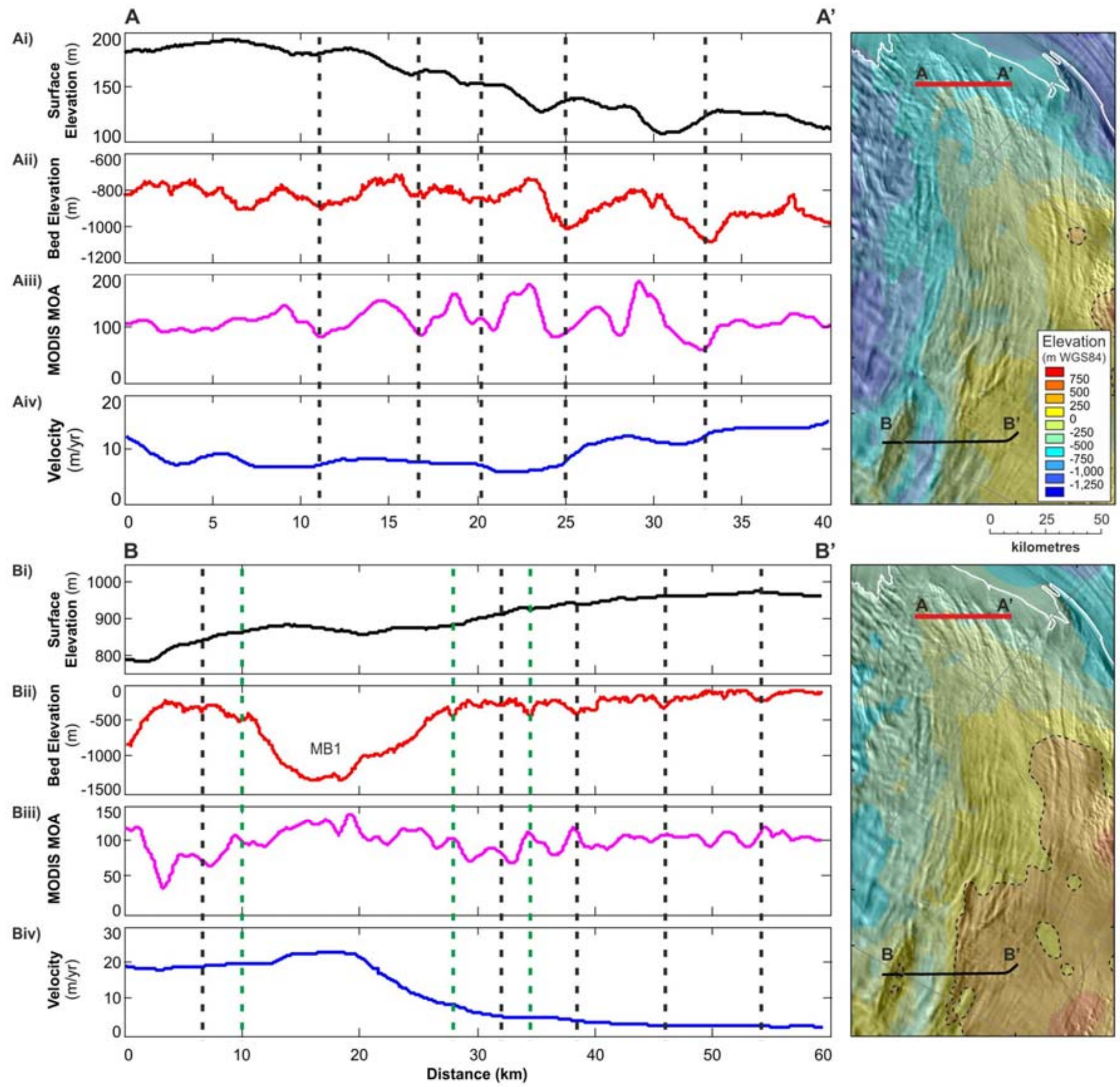

Figure DR2. Two transects taken along flightlines that cross a series of subglacial channels observed in RES data and satellite imagery in the region between the Möller and Foundation Ice Streams. **i,** Surface elevation. **ii,** Bed elevation. These are taken from the RES flightline data. **iii,** MODIS MOA satellite imagery (Haran et al., 2005, updated 2013). **iv,** Ice velocity (Rignot et al., 2011). These are sampled from grids. **A**: Flightline transect A-A' (red line) is located near the grounding line. **B**: Flightline transect B-B' (black line) is located further inland and crosses the northernmost (down glacier) Marginal Basin (Fig. 1C; Supplementary Fig. S1). Vertical black dashed lines mark the location of channels evident in the bed topography and at the ice sheet surface (Fig. 1C, white diamonds). Vertical green dashed lines mark the location of channels that are only evident in the bed topography (Fig. 1C, black diamonds). Inset: Present-day (upper) and rebounded (lower) bed elevations, overlain with a 0 m elevation contour, respectively (black dashed line), semi-transparent MODIS MOA imagery and associated grounding line (white line). Extent of inset is dashed black box in Fig. 1A.

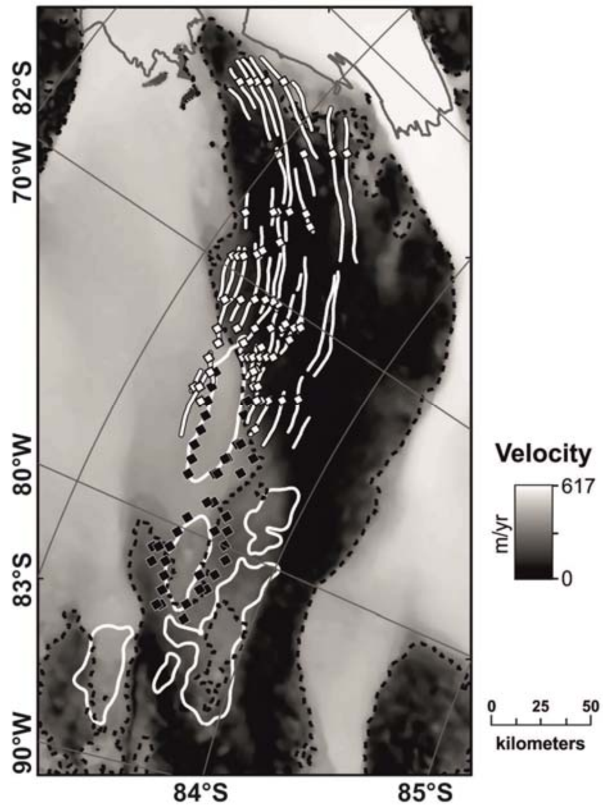

Figure DR3. Ice sheet velocity in the region of the Möller and Foundation Ice Streams, West Antarctica (Rignot et al., 2011). Dashed black line marks the 10 m a^{-1} contour. Grey line marks the MODIS MOA grounding line. White closed contours are the Marginal Basins (Fig. 1C). White lines show the location of channels observed in MODIS MOA imagery (Fig. 1B). White diamonds mark subglacial channels visible in both RES data and satellite imagery. Black diamonds mark subglacial channels only visible in RES data. Note: the surface expression of channels in the satellite imagery (white lines) closely corresponds with the 10 m a^{-1} velocity contour. Where ice sheet velocities are equal to or lower than this, the channels are evident in satellite imagery. Where ice sheet velocities exceed 10 m a^{-1} the channels are no longer visible at the ice surface.

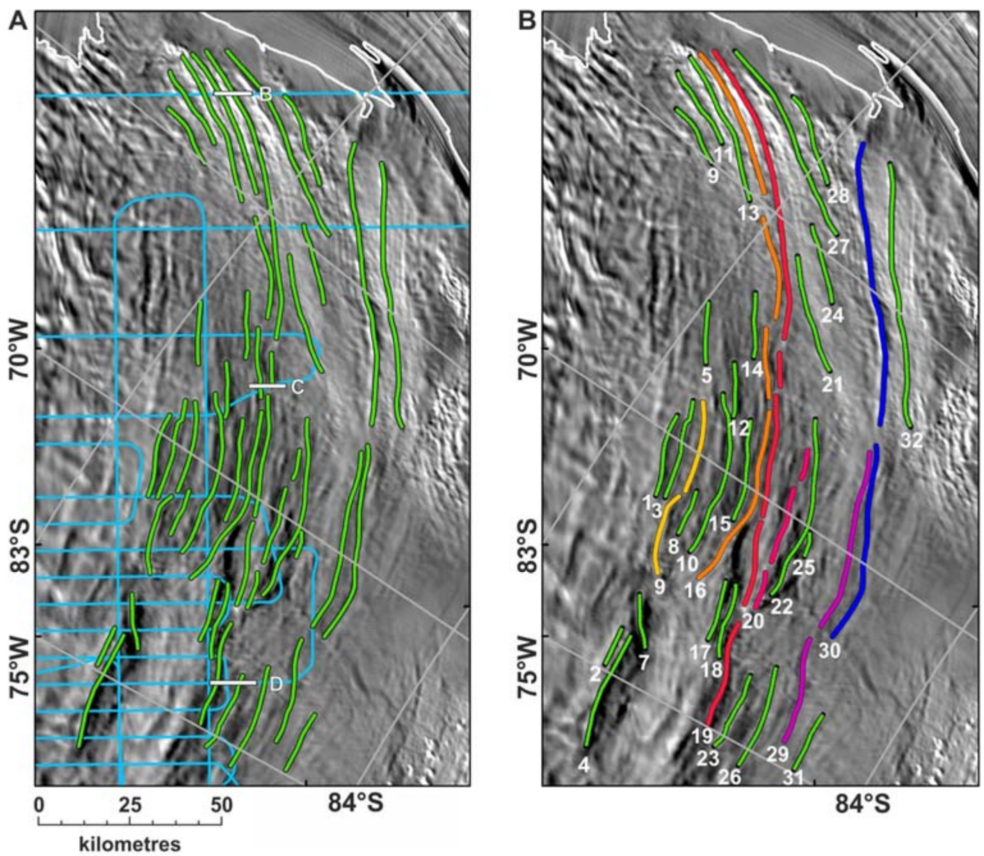

Figure DR4. Location and classification of channels observed in MODIS MOA imagery (Haran et al., 2005, updated 2013). Extent of panels is dashed black box in Fig. 1A. **A:** Green lines mark the location of 44 discontinuous channel segments identified in the MODIS MOA imagery. Blue lines represent flightlines, to show the spatial overlap between the two. Short white lines on the flightlines and lettering mark the locations of cross-profiles displayed in Fig. 2. **B:** For some channels and over short distances it was reasonable to extrapolate between channel segments with confidence and reclassify these segments as one channel (Supplementary Information #3). This resulted in the classification of a total of 32 single channels, labelled accordingly in this panel. To highlight where this occurred, those segments reclassified as a single channel are displayed in the same colour.

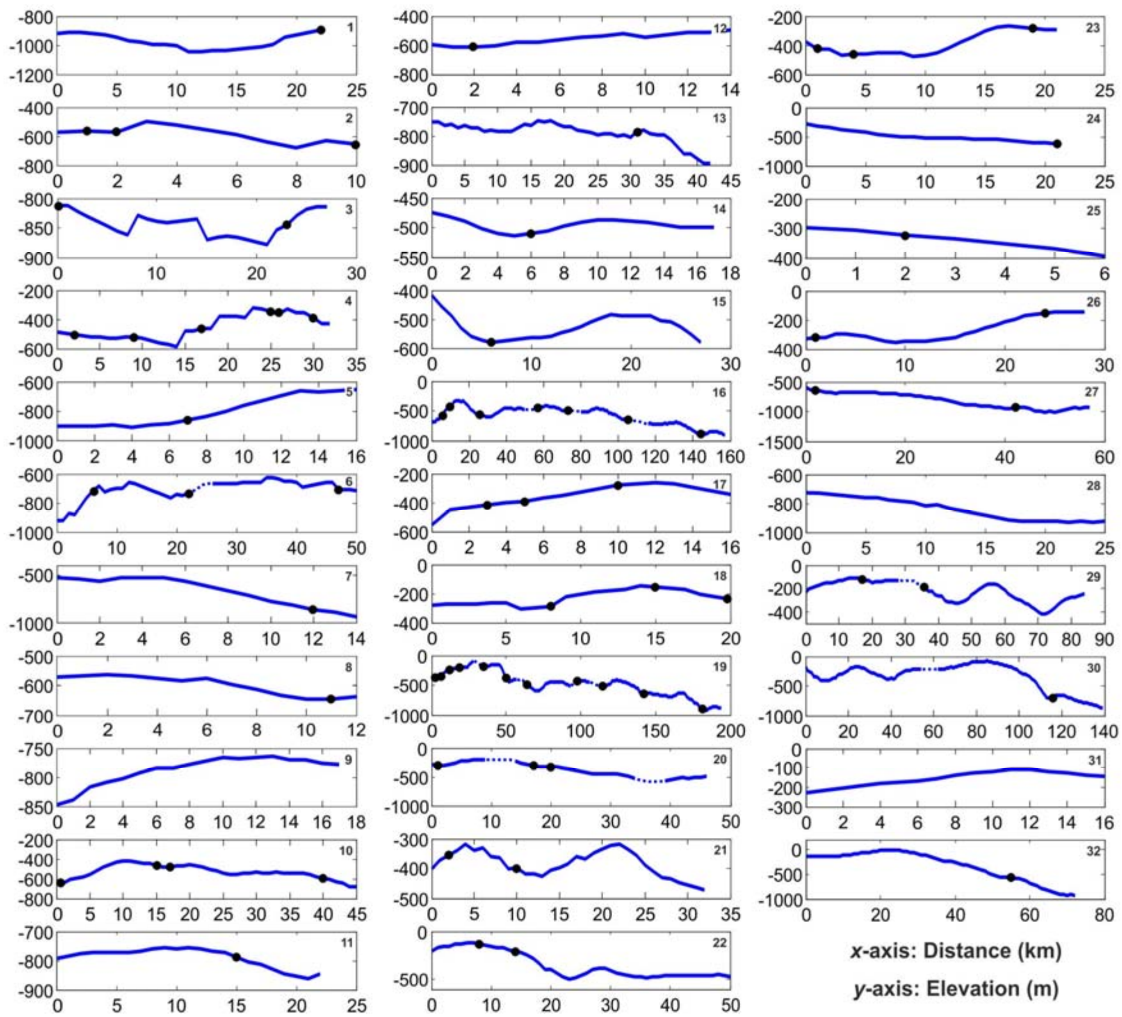

Figure DR5. Long-profiles of bed topography determined for the 32 channels identified in MODIS MOA imagery (Supplementary Fig. DR4). Elevations are derived from flightline data where channels intersected with flightlines (black dots) and elsewhere from the gridded bed topography (Supplementary Information #1 and 3). The long-profiles are numbered according to their corresponding channel segment detailed in Supplementary Fig. DR4B. Blue dashed lines mark extrapolated sections where channel segments were grouped into a single channel long-profile (i.e. channels 6, 16, 19, 20, 29 and 30). Note: the axes scales vary.

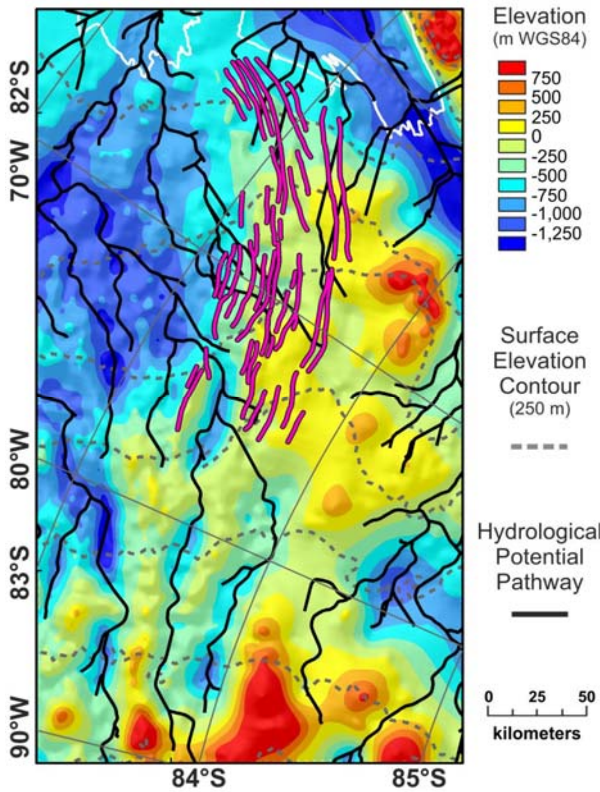

Figure DR6. Hydrological potential pathways and ice surface contours in the region of the Möller and Foundation ice streams, West Antarctica. Pathways (black lines) and surface contours (dashed grey lines, 250 m intervals) show where water would flow, if present beneath the ice sheet (Supplementary Information #4). Pink lines mark the location of channels observed in MODIS MOA satellite imagery (Fig. 1C). Channel orientations do not correspond with the direction of present-day hydraulic potential flow pathways and surface contours, indicating that they formed under a different ice sheet configuration and have since been preserved.

Table DR1. Example channel cross-profile dimensions and associated ice thicknesses. A total of 103 cross-profiles were identified in RES data. These are marked by the diamonds shown in Fig. 1C. This table presents the data for the 60 white diamonds, which mark where channels at the bed coincide with channels identified in the MODIS MOA imagery. The associated MODIS channel ID number (Supplementary Fig. S4B) is listed alongside the cross-profile ID number. More than one cross-profile is often found along the length of the MODIS channels. The cross-profiles displayed in Fig. 2 are identified with additional letters B, C, and D and highlighted in grey. They are found along channel 19 (Fig. 2E).

ID		Elevation (m)			Depth (m)		Width	
Cross-Profile	Channel	West	Mid	East	Minimum	Maximum	m	km
1	6	-832.3	-1103.7	-835.1	268.6	271.4	8067.3	8.1
2	10	-812.0	-1027.9	-753.3	215.9	274.6	6351.4	6.4
3	16	-745.5	-883.2	-793.7	89.5	137.7	4650.7	4.7
4	19	-780.3	-851.4	-720.5	71.1	130.9	2318.9	2.3
5	20	-741.9	-920.7	-779.8	140.9	178.8	5968.7	6.0
6	22	-620.0	-842.8	-648.4	194.4	222.8	5354.2	5.4
7	25	-570.2	-800.3	-625.5	174.8	230.1	4471.7	4.5
8	26	-499.0	-948.8	-448.8	449.8	500.0	4963.1	5.0
9	23	-574.7	-835.3	-628.3	207.0	260.6	2228.1	2.2
10	19	-356.7	-543.9	-439.0	104.9	187.2	2077.2	2.1
11 (D)	19	-436.6	-652.1	-473.5	178.6	215.5	3412.8	3.4
12	4	-527.6	-646.2	-526.8	118.6	119.4	2340.2	2.3
13	16	-528.8	-596.1	-513.4	67.3	82.7	1678.6	1.7
14	24	-778.2	-947.9	-790.1	157.8	169.7	3405.2	3.4
15	30	-857.3	-928.2	-823.0	70.9	105.2	997.8	1.0
16	32	-799.1	-913.8	-761.7	114.7	152.1	2926.7	2.9
17	27	-719.5	-828.7	-689.7	109.2	139.0	1563.8	1.6
18 (B)	19	-532.4	-653.1	-530.0	120.7	123.1	3293.8	3.3
19	16	-484.5	-519.2	-443.7	34.7	75.5	734.2	0.7
20	13	-420.5	-586.9	-452.7	134.2	166.4	1055.1	1.1
21	11	-225.3	-369.1	-184.1	143.8	185.0	2179.0	2.2
22	1	-549.9	-724.0	-542.6	174.1	181.4	2090.1	2.1
23	3	-566.8	-730.6	-550.7	163.8	179.9	1916.2	1.9
24	6	-513.5	-602.8	-430.0	89.3	172.8	1850.9	1.9
25	10	-424.1	-509.8	-460.1	49.7	85.7	2359.7	2.4
26	12	-596.6	-719.2	-607.5	111.7	122.6	2200.2	2.2
27	16	-722.3	-926.3	-695.2	204.0	231.1	2404.7	2.4
28	21	-728.2	-833.4	-690.8	105.2	142.6	2126.1	2.1
29	21	-575.2	-718.6	-544.4	143.4	174.2	2014.3	2.0
30 (C)	19	-510.8	-616.4	-491.9	105.6	124.5	3025.4	3.0

Table DR1 continued. Example channel cross-profile dimensions and associated ice thicknesses.

ID		Elevation (m)			Depth (m)		Width	
Cross-Profile	Channel	West	Mid	East	Minimum	Maximum	m	km
31	16	-450.3	-700.0	-484.5	215.5	249.7	3684.5	3.7
32	14	-284.1	-357.3	-285.2	72.1	73.2	2651.8	2.7
33	5	-159.6	-285.1	-132.6	125.5	152.5	2426.5	2.4
34	7	-207.8	-381.9	-252.4	129.5	174.1	1853.4	1.9
35	17	-960.7	-1163.0	-927.0	202.3	236.0	3553.6	3.6
36	17	-653.7	-822.8	-583.4	169.1	239.4	2353.2	2.4
37	17	-121.3	-233.9	-174.7	59.2	112.6	1139.9	1.1
38	18	-803.2	-1012.1	-703.8	208.9	308.3	4466.4	4.5
39	19	-611.4	-748.7	-493.8	137.3	254.9	3007.4	3.0
40	20	-451.6	-517.6	-372.5	66.0	145.1	1691.8	1.7
41	22	-212.8	-259.5	-206.6	46.7	52.9	642.6	0.6
42	20	-106.1	-259.7	-161.9	97.8	153.6	2799.0	2.8
43	19	-183.6	-389.7	-212.7	177.0	206.1	2156.9	2.2
44	16	-275.1	-401.9	-268.4	126.8	133.5	1781.3	1.8
45	15	-209.7	-392.5	-233.1	159.4	182.8	1554.6	1.6
46	10	-233.5	-419.3	-275.0	144.3	185.8	1213.6	1.2
47	8	-510.6	-556.8	-502.9	46.2	53.9	785.6	0.8
48	3	-478.8	-557.0	-441.4	78.2	115.6	718.6	0.7
49	2	-385.4	-457.7	-313.7	72.3	144.0	653.0	0.7
50	4	-239.3	-332.7	-231.8	93.4	100.9	1391.8	1.4
51	18	-274.5	-334.0	-290.9	43.1	59.5	420.0	0.4
52	19	-75.4	-235.0	-72.4	159.6	162.6	3738.7	3.7
53	6	-171.4	-334.0	-159.6	162.6	174.4	2097.5	2.1
54	16	-182.3	-413.0	-205.0	208.0	230.7	3766.6	3.8
55	18	-227.5	-455.4	-258.4	197.0	227.9	1502.4	1.5
56	18	-202.1	-316.1	-214.5	101.6	114.0	1706.2	1.7
57	18	-291.8	-391.1	-312.4	78.7	99.3	810.6	0.8
58	7	-263.5	-445.8	-278.5	167.3	182.3	2118.7	2.1
59	23	-459.4	-759.1	-271.7	299.7	487.4	3661.8	3.7
60	29	-359.4	-635.3	-362.3	273.0	275.9	4710.9	4.7
	Mean	-467.9	-622.5	-459.3	140.5	177.2	2584.7	2.6